IOP Publishing New J. Phys. 26 (2024) 033045 https://doi.org/10.1088/1367-2630/ad33cf

New Journal of Physics
The open access journal at the forefront of physics

Deutsche Physikalische Gesellschaft DPG
IOP Institute of Physics

Published in partnership with: Deutsche Physikalische Gesellschaft and the Institute of Physics

OPEN ACCESS

RECEIVED
15 November 2023

REVISED
7 March 2024

ACCEPTED FOR PUBLICATION
14 March 2024

PUBLISHED
26 March 2024

PAPER

Anomalies-Rich Floquet superconductivities induced by joint modulation of dynamic driving and static parameters

Donghao Wang[1], **Cong Cen**[1], **Liangliang Lu**[1], **Mengyao Li**[2], **Zixuan Ding**[1], **Yongchun Tao**[1,*] and **Jingguo Hu**[3]

[1] Department of Physics, Nanjing Normal University, Nanjing 210023, People's Republic of China
[2] College of Science, Nanjing Forestry University, Nanjing 210037, Jiangsu, People's Republic of China
[3] Department of Physics, Yangzhou University, Yangzhou 225009, People's Republic of China
[*] Author to whom any correspondence should be addressed.

E-mail: yctao88@163.com and jghu@yzu.edu.cn

Keywords: topological superconductors, Majorana fermions, topological phases of matter, Floquet systems, topological materials

Abstract

Current theoretical and experimental endeavors to realize an anomalous Floquet chiral topological superconductor (TSC), which is characterized by chiral Majorana edge modes independent of the Chern number, remain insufficient. Herein, we propose a new scheme that involves jointly tuning dynamic driving and static parameters within a magnetic topological insulator-superconductor sandwich structure to achieve this goal. The Josephson phase modulation induced by an applied bias voltage across the structure is utilized as a Floquet periodic drive. It is found that the interplay between the two kinds of tunings can bring about a lot more exotic Floquet TSC phases than those caused by only tuning the dynamic driving parameter (frequency ω or period τ). More importantly, just tuning static parameters (the chemical potential μ, Zeeman field g_z, and proximity-induced superconducting energy gap Δ_b) also can induce a series of novel topological phase transitions. Particularly, the features in the context of the three tunings are different from each other, originating from the combination of intrinsic and different extrinsic mechanisms. In addition, jointly tuning τ and μ (g_z) can have its own unique TSC phases. The proposed scheme should be readily accessible in experiments, and thus the family of anomalous Floquet TSC phases may be considerably enriched.

1. Introduction

In recent years, such well-known topological phases as Chern insulators [1, 2], topological insulators (TIs) [3–6], and topological superconductors (TSCs) [7–9] have been attracting an enormous amount of attention. Moreover, the non-Abelian Majorana zero modes connected intrinsically with the TSCs, have also stimulated tremendous research interest. The modes bridge between condensed matter physics and quantum computation [10–17].

Apart from static systems, topological phenomena also exist in systems far from equilibrium. A prototypical example is periodically driven systems that are described by Floquet theory [18–26]. Different parameters of the systems, such as chemical potential [27], external electromagnetic field [28], and system mass term [29], are modulated as periodic driving. Moreover, the combination of Floquet driving and different systems has induced rich physical properties. For example, novel topological phases are generated by the combination with Hermitian [30–33] and non-Hermitian systems [34–38]. Floquet systems could also be subjected to diverse potentials, such as tilted linear potential [39]and diagonal on-site potential in square lattice [40]. Floquet driving can be constructed upon different dimensional systems as well, such as one-dimensional (1D) and two-dimensional (2D) TSCs [41–45], forming higher-order topological phases with Majorana corner modes at 0 and π quasi-energies. For recent theoretical reviews, see [46–48].

Floquet engineering can enable nontrivial band topology in statically trivial systems and even achieve exotic topological phases without any static counterparts. Specifically, there may exist boundary modes in such Floquet systems as a 2D anomalous Floquet TI of the symmetry class A, which is of radical impossibility in static equilibrium systems [18, 20]. Even though all the corresponding Floquet bands are topologically trivial, the boundary is remarkably characterized by chiral topological modes just like a static Chern insulator. This has already been experimentally confirmed by the aid of ultracold atoms [49–51], photonic lattices [33, 52–61], and acoustic platforms [62, 63].

Unfortunately, there have been few efforts to address the corresponding superconducting counterpart except for only one very recent theoretical work [64]. A 2D anomalous Floquet chiral TSC with Chern-number-independent chiral Majorana edge modes (MEMs) was predicted. It is considered that such a Floquet TSC is generated entirely by the intrinsic dynamics arising from the dc-biased Josephson effect.

On the other hand, the chemical potential μ, Zeeman field g_z, and proximity-induced superconducting energy gap Δ_b have been found to exert significant influences on the realization of topological phases in low- and three-dimensional (3D) TSC structures.

A 1D Rashba nanowire, combined with proximity-induced *s*-wave superconductivity in the presence of Zeeman field g_z, is characterized by midgap Majorana modes (either chiral or non-chiral) on edges along and perpendicular to the wires [65]. At special values of g_z and μ, a phase with a single chiral MEM (analogous to a $p+ip$ superconductor [66, 67]) can be realized, which is almost completely localized at the outmost wires. The TSC phase can cover a broader chemical potential window in the existence of expulsive interactions, even without requiring g_z [68]. By simply tuning μ, ones can access three distinct phases, i.e. topologically trivial *s*-wave, topologically nontrivial $s_{\pm}$-wave, and nodal superconducting phases under impurity subgap states [69]. In the context of proximity-induced superconductivity induced by $s_{\pm}$-wave superconductor (SC), the evolution of the Majorana pair is caused by tuning g_z, leading to that the SC undergoes topological phase transitions [70]. Particularly, under a Floquet driving, regular 0- and anomalous π-Majorana end modes are generated by tuning μ and driving frequency ω [27]. Furthermore, non-Hermitian Floquet TSCs with multiple MEMs were proposed, which are based on a Kitaev chain with periodically kicked superconducting pairings and gain/losses in the chemical potential μ [38, 71].

An applied staggered Zeeman field g_z on the stacked tunnel-coupled 2D electron- and hole-gas layers with Rashba spin-orbit interaction can generate a second-order TI phase. It is characterized by the emergence of zero-mass hinge interfaces hosting chiral gapless hinge states, which is stable up to relatively large values of g_z [72]. In addition, for a 3D TI with bulk *s*-wave superconductivity under a perpendicular g_z, the Majorana states become more localized on a single surface with μ increased. However they spread into the bulk toward the opposite surface, and at μ being sufficiently high, the Majorana modes can tunnel between surfaces [73, 74].

It is then natural to ask whether the three static parameters μ, g_z, and Δ_b can exert significant influences on the realization of an anomalous Floquet chiral TSC in Floquet systems. So far, there has been a lack of systematic study on joint tuning of the dynamic driving and static parameters in Floquet TSC systems. And thus, the study is in need, which is the motivation of the present work.

In this work, we provide an affirmative answer to the above questions, based on a Floquet magnetic TI-based Josephson hybrid structure (see figure 1(a)). The static bias voltage applied across the top and bottom SC layers offers a driving protocol for the setup (the Josephson phase, i.e. the relative phase between the SCs as a periodic function of time). By jointly tuning the dynamic driving parameter (frequency ω or period τ) and one of static parameters μ, g_z, and Δ_b, (see figure 1(b)), a variety of anomalies-rich Floquet TSC phases are exhibited, most of which are not shown in [64]. In the low frequency ω or large driving period τ region, for different μ, different novel Floquet topological phase transitions will occur sequentially as τ increases, also indicating a series of topological phase transitions at a fixed τ induced by μ. And the same features are found for different g_z and Δ_b. Particularly, there always exist several special values for μ, g_z, and Δ_b, respectively, at two any adjacent values of which, the corresponding topological phases appearing successively with the increase of τ are thoroughly different. This also indicates a series of topological phase transitions in the whole τ region tuned by μ, g_z, and Δ_b, respectively. Remarkably, with the enhancement of μ and Δ_b, the numbers of the topological phases arising successively tuned by τ may both increase or decrease, while the number basically enhances with g_z. More interestingly, for tuning both μ and g_z, there are unique TSC phases, however, for tuning Δ_b, all the topological phases have appeared in those for tuning μ and g_z. In addition, a total of up to 19 different topological phases are exhibited, which considerably enriches the family of anomalous Floquet TSC phases.

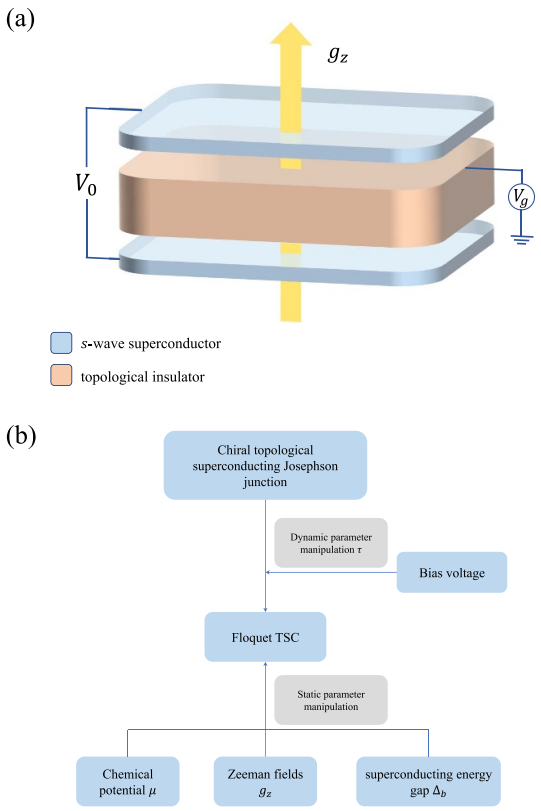

Figure 1. (a) Schematic diagram of a Floquet sandwich-like TI Josephson hybrid structure, where the middle layer is a TI, and the top and bottom layers are s-wave SCs. A Zeeman field g_z along the z direction is applied to make the TI become a 3D magnetic one. Two gate voltages V_g applied on the top and bottom surfaces of the TI can adjust the chemical potential μ. A periodic phase concerned with a bias voltage V_0 between the two s-wave SC layers is used as a Floquet period drive, leading to the Josephson junction transformed into a Floquet TSC. (b) Tuning the driving period τ by varying the bias voltage V_0 allows for dynamic modulation of the Floquet TSC phase. Meanwhile, the Floquet TSC phase is subject to the manipulation of the static parameters (chemical potential μ, Zeeman field g_z, and proximity-induced superconducting energy gap Δ_b).

2. Model Hamiltonian and Floquet theory

Consider a chiral topological Josephson hybrid structure with a magnetic (Cr-doped [75]) 3D TI sandwiched in between the top and bottom s-wave SCs. In the structure, the Zeeman field along the z direction, bias voltage V_0 between the top and bottom s-wave SC layers, and gate voltage V_g on both the top and bottom surfaces of the 3D magnetic TI, are applied as shown in figure 1(a). The BdG (Bogoliubov-de Gennes) Hamiltonian of the structure is written as [76–78]

$$H(\mathbf{k},t)=\begin{bmatrix} h_{\mathrm{MTI}}(\mathbf{k})-\mu & h_{\Delta}(t) \\ h_{\Delta}^{\dagger}(t) & -h_{\mathrm{MTI}}^{T}(-\mathbf{k})+\mu \end{bmatrix} \tag{1}$$

with the Hamiltonian of the magnetic TI
$h_{\mathrm{MTI}}(\mathbf{k})=v(\sin k_x\sigma_z\bigotimes s_y-\sin k_y\sigma_z\bigotimes s_x)+t(\mathbf{k})\sigma_x\bigotimes s_0+g_z\sigma_0\bigotimes s_z$ and

$$h_{\Delta}(t)=\begin{bmatrix} -i\Delta_t e^{i\varphi(t)}s_y & 0 \\ 0 & -i\Delta_b s_y \end{bmatrix}. \tag{2}$$

Here σ and s are the the Pauli matrices denoting the surface layer and spin degrees of freedom, respectively, μ is the chemical potential, $t(\mathbf{k})=t_0-t_1(\cos k_x+\cos k_y)$ describes the hybridization between the top and bottom Dirac surface states of the 3D magnetic TI, and g_z represents the Zeeman field. In equation (2), the pairing potentials of the top and bottom SCs respectively given by $\Delta_{t,b}$, are assumed identical, and $\varphi(t)$ stands for the Josephson periodic phase $\varphi(t)=\varphi_0+2eV_0t$ as a periodic driving with the frequency $\omega=2eV_0$.

The time-dependent Hamiltonian is needed to convert into a Floquet frequency- or period-dependent one, which is infinite-dimensional and truncated appropriately for numerical calculations. Its matrix elements are given by the following formula [79],

$$(H_F)_{nm}=h_{\omega}^{n-m}+\omega n\delta_{nm}, n,m\in\mathbb{Z} \tag{3}$$

with

$$h_{\omega}^{n-m}=1/\tau\int_{0}^{\tau}H(t)\,\mathrm{e}^{i(n-m)\omega t}\mathrm{d}t, \tag{4}$$

where

$$\begin{aligned}h_{\omega}^{(0)}&=H(\mathbf{k},t)\,(\Delta_t\to 0)\,,\\ h_{\omega}^{(1)}&=\frac{\Delta_t}{2}\left(\tau_y\bigotimes\sigma_+\bigotimes s_y-i\tau_x\bigotimes\sigma_+\bigotimes s_y\right),\end{aligned} \tag{5}$$

$h_{\omega}^{(-1)}=(h_{\omega}^{(1)})^{\dagger}$, and $\sigma_{\pm}=(\sigma_0\pm\sigma_z)/2$. For the matrix elements with $|n-m|>1$, the presence of $\mathrm{e}^{i(n-m)\omega t}$ in equation (4) makes the integration result over the entire period τ naturally equal to 0.

The BdG Chern number $\mathcal{C}$ is defined by using the following formula [80]

$$\mathcal{C}=\sum_{n}C_n, \tag{6}$$

where all the quasi-energy bands lying between $(0,\omega/2]$ are involved and

$$C_n=\frac{1}{2\pi}\int_{\mathrm{BZ}}\mathrm{d}\mathbf{k}^2\Omega_n(\mathbf{k}) \tag{7}$$

with the integral over the complete Brillouin zone. In equation (7), $\Omega_n(\mathbf{k})$ the Berry curvature can be expressed as a summation of eigenstates

$$\Omega_n(\mathbf{k})=i\sum_{n'\neq n}\frac{\langle n|\frac{\partial H}{\partial k_x}|n'\rangle\langle n'|\frac{\partial H}{\partial k_y}|n\rangle-\left(k_x\leftrightarrow k_y\right)}{\left(\varepsilon_n-\varepsilon_{n'}\right)^2}. \tag{8}$$

Here, the obtained $\mathcal{C}$ for a 2D anomalous Floquet chiral TSC with Chern-number-independent chiral MEMs is, in general, clearly distinguished from that for the conventional Floquet chiral TSC. The latter is like the one in the high-frequency limit, which is adiabatically equivalent to a static chiral TSC with the same $\mathcal{C}$. Besides, $\mathcal{C}$ is based on the Floquet theory, which converts the time-dependent Hamiltonian into a frequency-dependent one. We use a truncated Floquet Hamiltonian H_F, and integrate over the entire Brillouin zone to obtain $\mathcal{C}$. This process only requires static calculations without involving time integration.

For the chiral MEMs in such a 2D anomalous Floquet chiral TSC, a relevant topological invariant, i.e. a homotopy-based winding number, is needed to deliberately describe them [18, 20, 22, 81–83]

$$\begin{aligned}\mathcal{W}=\frac{1}{8\pi^2}\int_0^{\tau}\mathrm{d}t\iint_{\mathrm{BZ}}\mathrm{d}\mathbf{k}\mathrm{Tr}\Big\{&\left(U_{\epsilon}(\mathbf{k},t)^{-1}\partial_t U_{\epsilon}(\mathbf{k},t)\right)\\ &\times\left[\left(U_{\epsilon}(\mathbf{k},t)^{-1}\partial_{k_x}U_{\epsilon}(\mathbf{k},t)\right),\left(U_{\epsilon}(\mathbf{k},t)^{-1}\partial_{k_y}U_{\epsilon}(\mathbf{k},t)\right)\right]\Big\}\end{aligned} \tag{9}$$

with $U_{\epsilon}(\mathbf{k},t)=U(\mathbf{k},t)[U(\mathbf{k},\tau)]_{\epsilon}^{-\frac{t}{\tau}}$. In equation (9), the time-evolution unitary $U(\mathbf{k},t)=\mathcal{TO}$ $\exp[-i\int_0^t H(\mathbf{k},t)\mathrm{d}t]$ with $\mathcal{TO}$ denonting the time ordering and [84]

$$[U(\mathbf{k},\tau)]_{\epsilon}^{-\frac{t}{\tau}}=\sum_{m=1}^{N}\exp\left[-\frac{t}{\tau}\log_{\epsilon}\left(\mathrm{e}^{-i\varepsilon_m}\right)\right]P_{\mathbf{k},m}(\tau) \tag{10}$$

with m representing the band index and $P_{\mathbf{k},m}(\tau)$ the projection matrix given by the eigenvector of $U(\mathbf{k},\tau)$ for $\mathrm{e}^{-i\varepsilon_m}$. Here, $\mathrm{e}^{-i\varepsilon_m}$ denotes the m-th eigenvalue of $U(\mathbf{k},\tau)$, the summation in equation (10) extends over all eigenvalues, and ϵ serves as the branch cut of the logarithm by requiring $i\log_{\epsilon}(x)\in[\epsilon,\epsilon+2\pi)$ for all $x\in U(1)$. As we always set the branch cut to $\epsilon=-\pi$, we have

$$i\log_{\epsilon}\left(\mathrm{e}^{-i\varepsilon_m}\right)=\varepsilon_m. \tag{11}$$

For the calculation of $\mathcal{W}$, the integrations over not only the Brillouin zone but also time covering a complete driving period, are required, which is much different from the situation for calculation of $\mathcal{C}$. Therefore, when calculating $\mathcal{W}$, we use the original time-dependent Hamiltonian $H(\mathbf{k},t)$, and a time evolution operator with periodic invariance $U_{\epsilon}(\mathbf{k},t)$, which satisfies $U_{\epsilon}(\mathbf{k},t)=U_{\epsilon}(\mathbf{k},t+\tau)$.

The values of both $\mathcal{C}$ and $\mathcal{W}$ determine the specific form of bulk-edge correspondence. In the quasi-one-dimensional spectrum, edge states can appear in the gaps at $E=0$ and/or $\omega/2$. The number of

edge states in the gap at $\omega/2$ is indicated by $\mathcal{W}$, while the one in the gap at $E=0$ is just the sum of $\mathcal{C}$ and $\mathcal{W}$. Therefore, different combinations of $\mathcal{C}$ and $\mathcal{W}$ represent different topological phases. For the two topological phases with the same $\mathcal{W}$, they also have the same number of edge states in the gap at $\omega/2$. However, for the two topological phases with the same $\mathcal{C}$ but different $\mathcal{W}$, they possess different numbers of edge states in the gaps at both $E=0$ and $\omega/2$. Specifically, in the gap at $E=0$, for the driving period τ within high-frequency limit, the number of edge states is only dependent on $\mathcal{C}$ due to $\mathcal{W}=0$, while for τ beyond the limit, relies on both $\mathcal{C}$ and $\mathcal{W}$. A detailed analysis will be performed by combining the specific edge states and topological phases in the subsequent sections.

3. Results and discussions

With the gradual diminishment of V_0 from the high-frequency limit, Floquet TSC states with chiral MEMs across the $E=\omega/2$ energy gap are generally expected to produce, accompanied by Floquet topological phase transitions. The Floquet TSC states are generated entirely by the intrinsic dynamics in the present Josephson hybrid structure, even with the starting from the topologically trivial state ($\mathcal{C}=0$), as shown in the following. The corresponding topological phase transitions are modulated by Josephson phase through simply changing the bias voltage V_0. The dynamic driving (tuning frequency ω or period τ) is necessary to produce the topological phase transitions, which is intrinsic. However, the possible results of topological phase transitions are also sensitively dependent on static parameters (e.g. μ, g_z, and Δ_b, etc). Specifically, only for proper static parameters, can the Floquet TSC states be induced, which is extrinsic. In the following, therefore, we investigate the Floquet TSC phases and corresponding phase transitions tuned jointly by dynamic driving (ω or τ) and static (μ, g_z, and Δ_b) parameters.

3.1. Topological phase transitions tuned jointly by chemical potential and driving period

In this section, we present anomalies-rich Floquet chiral TSC phases with Chern-number-independent chiral MEMs, which are tuned simultaneously by chemical potential μ and driving period τ.

Table 1 shows the topological phase diagram, the topological phase transitions as a function of μ and τ. It is divided into areas 1, 2, and 3 according to the different topological phases in the high-frequency limit region. At the high-frequency limit, the phase transitions from $\mu=0.3$ to 0.4 and from $\mu=0.9$ to 1 are due to the closures of the bulk energy bands at $\mathrm{X}(\pi,0)$ and $\mathrm{M}(\pi,\pi)$, respectively.

In area 1, when μ is slightly increased, e.g. $\mu=0.1$, the topological phases appearing sequentially with the increase of driving period τ keep unchanged, including the corresponding driving period regions. This also indicates that there exists no topological phase transition tuned by μ at any fixed τ. It follows that for joint tuning of the dynamic driving and static parameters, the former thoroughly predominates over the latter. With the further increase of μ, e.g. $\mu=0.2$, the topological phases arising successively with τ still keep constant in the range for small τ (from 0 to 2.2), while are thoroughly different in the range for big τ (from 2.3 to 2.6). Specifically, for the latter range, the order of the topological phases occurring successively with τ is the three phases $(0,1)$, $(2,-1)$, and $(3,-2)$, replacing the two phases $(3,-2)$ and $(2,-1)$ at $\mu=0.1$. This indicates the thoroughly different topological phase transitions with τ and several ones at fixed periods τ tuned by μ. As μ is continuously enhanced, e.g. $\mu=0.3$, the order of the topological phase appearing sequentially with τ in the range for small τ (from 0 to 2.3) keeps unchanged. Yet the period region corresponding to each phase is considerably different from that at $\mu=0.2$, which means possible topological phase transitions with μ at some τ. Particularly, in the range for big τ (from 2.3 to 2.6), the order of $(0,1)$, $(2,-1)$, and $(3,-2)$ is replaced by the one of $(0,1)$, $(3,-2)$, and $(4,-2)$, where $(4,-2)$ is a new phase. And thus, the thoroughly different topological phase transitions with τ emerge. It also follows that in the region for the big τ, the topological phase transitions at a fixed τ tuned by μ from 0.2 to 0.3 appear. Therefore, tuning μ in the range of small μ exerts a significant influence on producing the new topological phases only at the range of big τ, as seen in table 1. There are six kinds of phases, i.e. $(1,0)$, $(0,1)$, $(-1,2)$, $(2,-1)$, $(3,-2)$, and $(4,-2)$ in this area.

When μ is increased into area 2, a variety of new topological phases thoroughly different from those in area 1, start to emerge. For example, at $\mu=0.4$, the order of $(-1,0)$, $(-2,1)$, $(0,-1)$, $(-1,0)$, $(-2,1)$, $(-1,0)$, and $(0,0)$ is presented. This implies the entirely new phase topological transitions modulated by not only τ but also μ from $\mu=0.3$ to 0.4 (between the adjacent areas) at any fixed τ. Similarly, in this area, when μ is slightly increased, e.g. $\mu=0.5$, the topological phases emerging successively with the increase of τ keep unchanged. However, each corresponding driving period region varies except for the high-frequency limit region, indicating that the topological phase transitions with μ from 0.4 to 0.5 can appear at most fixed τ. With the further increase of μ, e.g. $\mu=0.6$, there still exist five topological phases, and the order of the former four ones keeps the same, but the corresponding driving period regions are much different. And then, with each increment of 0.1 in μ from 0.6 to 0.9, one more topological phase emerges as τ grows. The

Table 1. The topological phase diagram tuned jointly by dynamic driving and static parameters (τ and μ), where each phase is labeled by two integer-valued topological invariants, BdG-Chern number and winding number, written as $(\mathcal{C},\mathcal{W})$. The phase diagram is divided into areas 1 (blue), 2 (green), and 3 (orange) according to the different topological phases in the high-frequency ω (small τ) limit. Here, $g_z = 0.6$ and $\Delta_b = 0.4$.

τ \ μ	0	0.1	0.2	0.3	0.4	0.5	0.6	0.7	0.8	0.9	1
0.1	1,0	1,0	1,0	1,0	-1,0	-1,0	-1,0	-1,0	-1,0	-1,0	0,0
0.2											
0.3											
0.4											
0.5											
0.6											
0.7											
0.8											
0.9											
1											
1.1									-2,1	-2,1	-1,1
1.2							-2,1	-2,1			
1.3				0,1	-2,1	-2,1				0,-1	1,-1
1.4	0,1	0,1	0,1					0,-1	0,-1		
1.5							0,-1			-1,0	0,0
1.6									-1,0		
1.7	-1,2	-1,2	2,-1	2,-1	0,-1	0,-1		-1,0		0,-1	1,-1
1.8	1,0	1,0	1,0	1,0	-1,0	-1,0	-1,0		0,-1		
1.9								0,-1			2,-1
2					-2,1	-2,1			1,-1	1,-1	
2.1											0,1
2.2				0,1	-1,0	-1,0	0,0	0,0	0,0	-1,1	-2,1
2.3	3,-2	3,-2	0,1								
2.4	2,-1	2,-1	2,-1	3,-2	0,0	0,0				-4,2	-3,1
2.5			3,-2	4,-2							
2.6											

former several phases are always identical and have the same order. Nevertheless, their corresponding driving period regions are much different for different μ. Particularly, the two new topological phases $(1,-1)$ at $\mu = 0.8$ and 0.9 as well as $(-4,2)$ at $\mu = 0.9$ are exhibited. All these mean that a variety of new topological phase transitions manipulated jointly by μ and τ take place in area 2. In this area, there are seven kinds of phases, i.e. $(-1,0)$, $(-2,1)$, $(0,-1)$, $(0,0)$, $(1,-1)$, $(-1,1)$, and $(-4,2)$, which are thoroughly from those in area 1, in particular, the range of μ corresponding to area 2 is comparatively wide.

With μ increased into area 3, e.g. $\mu = 1$, there are nine topological phases arising sequentially with τ, which are thoroughly different from those at $\mu = 0.9$, indicating different novel topological phase transitions by not only τ but also μ at any fixed τ. There are seven kinds of phases, i.e. $(0,0)$, $(-1,1)$, $(1,-1)$, $(2,-1)$, $(0,1)$, $(-2,1)$, and $(-3,1)$ in this area.

From what has been observed above, it is concluded that just tuning static parameter μ always induces a series of novel topological phase transitions at any fixed τ between the adjacent areas. This also suggests that as long as the topological phase transitions at a fixed high-frequency ω (small τ) limit tuned by μ appear, the ones at a fixed big τ will take place. The reason can be explained by the combination of intrinsic and extrinsic mechanisms as follows. As τ increases, the reason for the topological phase transition is that the energy gap of the Floquet bulk energy band at $E = \omega/2$ is in turn closed. The point for the energy gap closure lies at the high symmetry point of the Brillouin zone (see figure 2). The variable spacing between the gap closure points leads to a wide or narrow range of driving periods for different topological phases. We only consider the gap at the high-symmetry point because it is the crucial indicator of the topological phase transition. More specifically, when the topological phase transition takes place, the gap at the high-symmetry point closes first, and then the closing point opens again with the increase of τ, forming a new topological phase. Until the gap at the next high-symmetry point closes, the topological phase will not change again.

When τ is relatively large, the Floquet bulk energy band is also deformed by adjusting μ, and this deformation changes the order in which the high symmetry points intersect with the $E = \omega/2$ line. For example, the third topological phase from $\mu = 0.1$ to 0.2 undergoes a band deformation, causing the topological phase transition from $(-1,2)$ to $(2,-1)$ at a fixed τ. This results in that intersecting of $E = \omega/2$ line with energy band of $h_\omega^{(0)}$ changes from at the high-symmetry X point first (see figure 2(a)) to at the M point first (see figure 2(b)).

In addition, with the change of μ, there is another kind of topological phase transitions due to the closure of the high symmetry point of the bulk energy band near $E = 0$. For example, in the range of μ from 0.3 to 0.42 (see figures 3(a)–(c)), with the increase of μ, the bulk energy band at the high symmetry point $\mathrm{X}(\pi,0)$ first opens, then closes and lastly opens. Resultantly, the system is driven into the topological phase transition, making the Chern number $\mathcal{C}$ of the system change from 1 to -1. At the boundaries between different areas, these two types of transitions often interact together. That is, the energy gap closes at both $E = 0$ and $\omega/2$, which leads to completely different topological phases under modulation of μ at the adjacent boundaries of two areas.

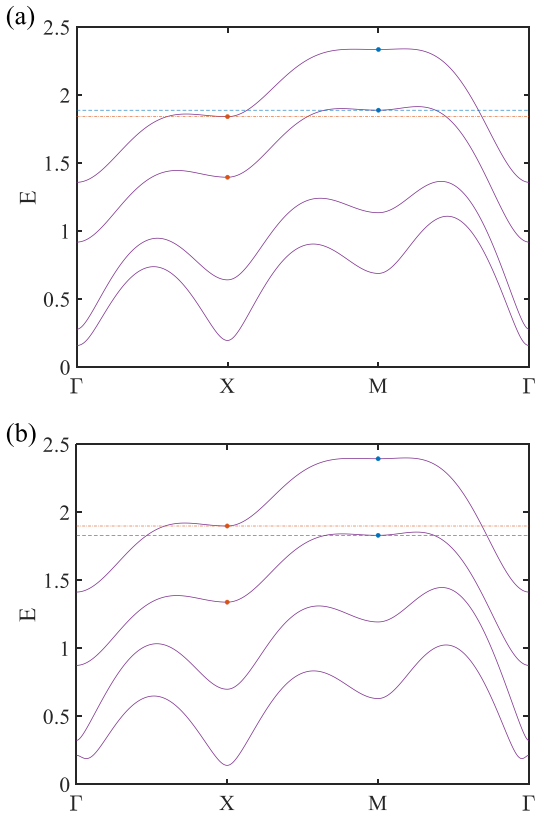

Figure 2. Different chemicals $\mu = 0.1$ (a) and 0.2 (b) lead to intersecting of the $E = \omega/2$ lines (e.g. the two lines marked by the dash-dot and dash ones) with the static bands $h_\omega^{(0)}$ at different high-symmetry points. Here, only the upper half spectrum is presented for simplicity and the other parameters are $\Delta_b = 0.4$ and $g_z = 0.6$.

The general relation between the bulk topological indices $(\mathcal{C}, \mathcal{W})$ and edge Majorana physics can be understood as follows. Let us first denote the numbers of chiral MEMs within the $E = \gamma$ gap as $n_{\text{edge}}(\gamma)$ for $\gamma = 0, \omega/2$, where the positive (negative) $n_{\text{edge}}(\gamma)$ stands for the number of right- (left-) shifted chiral MEMs. Then the bulk-edge correspondence is given by [49, 64]

$$n_{\text{edge}}(0) = \mathcal{C} + \mathcal{W}, n_{\text{edge}}\left(\frac{\omega}{2}\right) = \mathcal{W}. \tag{12}$$

The bulk-edge correspondence can be exemplified by the bulk quasi-energy bands or the edge state of the anomalous Floquet chiral TSC phase $(\mathcal{C}, \mathcal{W}) = (1, -1)$ at $\tau = 1.9$ and $\mu = 1$ as shown in figure 4. It is found that no edge state is generated at $E = 0$ (see figure 4(a)), but there exist two edge modes or a pair of modes (near the two edges $n = 0$ and 100) at $E = \omega/2$ (see figure 4(b)), which are respectively given by the red and black lines. For each mode at $E = \omega/2$, there is left- or right-shifted chirality, e.g. the edge mode corresponding to the red line, belongs to the former. Obviously, the total number of edge modes agrees with equation (12). The distributed probabilities at the blue circle on the left-shifted chiral edge state at $E = \omega/2$ are shown in figure 4(c), from which we can demonstrate that the chiral MEM indeed locates near the boundary with $n = 100$.

3.2. Topological phase transitions regulated jointly by Zeeman field and driving period

In this section, we illustrate the anomalies-rich Floquet chiral TSC phases with Chern-number-independent chiral MEMs tuned jointly by Zeeman field g_z and driving period τ.

Table 2 shows the topological phase diagram, the topological phase transitions as a function of g_z and τ. It is divided into four areas 1, 2, 3, and 4 according to the topological phase of the high-frequency limit region. At the high-frequency limit, the phase transitions tuned by g_z from 0.3 to 0.4 and from 0.7 to 0.8 are both due to the closure of the bulk energy band at $\Gamma(0, 0)$, while the one from 0.8 to 0.9 stems from the closure at $\mathrm{X}(\pi, 0)$.

In area 1, when g_z is slightly increased, the topological phases emerging sequentially with the increase of τ have a great change. Specifically, there exist four topological phases appearing successively at $g_z = 0.1$ but three ones at $g_z = 0.2$. Although the former two phases are the same for both cases, the corresponding period regions are much different from each other. Particularly, the latter two phases at $g_z = 0.1$ are $(0, 0)$ and

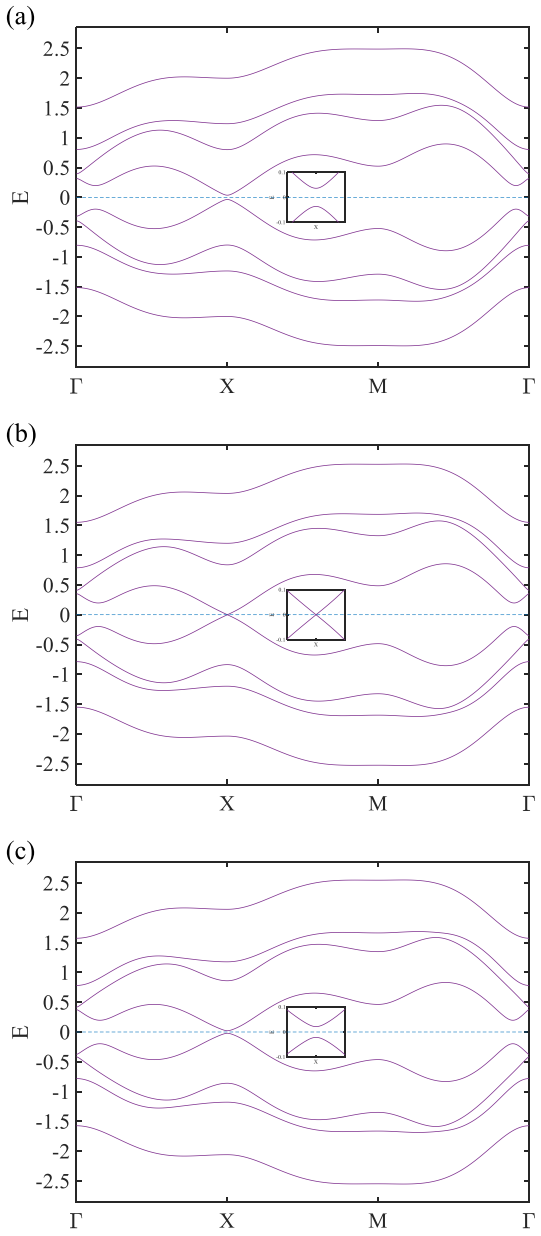

Figure 3. The evolution of the bulk energy band near $E = 0$ induced by μ, which is exemplified by $\mu = 0.35$ (a), 0.394 (b), and 0.42 (c). The other parameters are the same as in figure 2.

$(2, -2)$, which are thoroughly from the latter one at $g_z = 0.2$. These indicate not only the new different phase transitions tuned by τ in the range for big τ between each other but also the phase transitions tuned by g_z from 0.1 to 0.2 at most fixed τ. Thus, the features are much different from those with varied μ from the beginning in table 1. With the further increase of g_z from 0.2 to 0.3, the topological phases arising successively with τ keep unchanged, but the corresponding driving period regions change greatly, which indicates that there exist topological phase transitions tuned by g_z at some fixed τ. In this area, there exist four kinds of different topological phases, i.e. $(0, 0)$, $(1, -1)$, $(-1, 1)$, and $(2, -2)$.

As in table 1 for tuning μ, with g_z increased into area 2, a variety of new topological phases thoroughly different from those in area 1, start to emerge, e.g. at $g_z = 0.4$, in the order of the five phases $(1, 0)$, $(0, 1)$, $(-1, 2)$, $(1, 0)$, and $(2, -1)$. This indicates not only the entirely new topological phase transitions tuned by τ but also the topological phase ones induced by g_z from 0.3 to 0.4 at any fixed τ between the adjacent two areas. With g_z increased to 0.5, the former four topological phases occurring sequentially with the increase of τ, including the order, keep unchanged, and only the last one is $(3, -2)$ replacing $(2, -1)$ at $g_z = 0.4$. But the corresponding driving period regions change greatly except for the high-frequency limit. Thus, not only is the last phase transition tuned by τ different, but also the phase transition modulated by g_z can take place at most fixed τ. And then, as g_z increases gradually from 0.5 to 0.7, the number of topological phases that appear in sequence with the rising τ also increases by one. The former five phases are always identical and

Table 2. The same as in table 1 except that μ is replaced by g_z and the topological diagram is divided into areas 1 (blue), 2 (green), 3(orange), and 4 (purple). Here, $\mu = 0$ and $\Delta_b = 0.4$.

τ \ g_z	0.1	0.2	0.3	0.4	0.5	0.6	0.7	0.8	0.9	1	1.1
0.1	0,0	0,0	0,0	1,0	1,0	1,0	1,0	2,0	0,0	0,0	0,0
0.2											
0.3											
0.4											
0.5											
0.6											
0.7											
0.8											
0.9											
1											
1.1											
1.2										-1,1	-1,1
1.3								1,1	-1,1		
1.4						0,1	0,1			-2,2	0,0
1.5				0,1	0,1			0,2	0,0	0,0	
1.6			-1,1			-1,2	-1,2	2,0			2,-2
1.7		-1,1		-1,2	-1,2		1,0		2,-2	2,-2	1,-1
1.8	-1,1			-1,2		1,0		4,-2		1,-1	
1.9					1,0		3,-2		1,-1		2,-1
2				1,0		3,-2		3,-1		2,-1	1,0
2.1	0,0		1,-1		1,0		2,-1		2,-1		
2.2		1,-1		2,-1		2,-1		2,-1		1,0	
2.3					3,-2		3,-1		1,0		2,0
2.4											
2.5	2,-2										
2.6											

have the same order, however, their corresponding driving period regions are much different for different g_z. Particularly, the two new topological phases $(2,-1)$ at $g_z = 0.6$ and 0.7 as well as $(3,-1)$ at $g_z = 0.7$ are exhibited. All these mean that a variety of new topological phase transitions tuned by both g_z and τ take place in area 2. There are six kinds of phases in this area, i.e. $(1,0)$, $(0,1)$, $(-1,2)$, $(2,-1)$, $(3,-2)$, and $(3,-1)$, which are thoroughly different from those in area 1.

With g_z increased into area 3, e.g. $g_z = 0.8$, there are still seven topological phases occurring sequentially, but they are thoroughly different from those in the former two areas. As a result, different novel topological phase transitions tuned by τ are produced and there exist the topological phase transitions manipulated by g_z at almost all τ. In this area, there are four kinds of phases, i.e. $(2,0)$, $(1,1)$, $(0,2)$, and $(4,-2)$, which are not exhibited in the former two areas.

More interestingly, when g_z is slightly increased, e.g. $g_z = 0.9$, area 4 just turns up. There still exist seven topological phases arising successively, but they are much different from those at $g_z = 0.8$. There exist eight topological phases appearing sequentially at both $g_z = 1$ and 1.1. Only the third phase $(-2,2)$ at $g_z = 1$ and the last phase $(2,0)$ at $g_z = 1.1$ are added, respectively, but the order for other phases is the same as the one at $g_z = 0.9$. Thus two new phase transitions tuned by τ from $(-1,1)$ to $(-2,2)$ and from $(-2,2)$ to $(0,0)$ at $g_z = 1$, replace the one $(-1,1)$ to $(0,0)$ at $g_z = 0.9$. Another new one tuned by τ from $(1,0)$ to $(2,0)$ at $g_z = 1.1$, is produced. However, similarly due to the corresponding driving period region for each phase varying with g_z, the phase transitions tuned by g_z at a fixed τ can appear. In this area, there is a new phase $(-2,2)$, which is never exhibited in the former areas.

From the above, we observe that not only the six new topological phases $(1,1)$, $(0,2)$, $(2,0)$, $(2,-2)$, $(-2,2)$ and $(3,-1)$ but also some exotic topological phase transitions in table 2 are never exhibited in table 1.

Now, take the phase $(\mathcal{C},\mathcal{W}) = (0,0)$ in table 2 with $\tau = 1.6$ and $g_z = 1$ as an instance to illustrate the bulk energy bands or the edge state of the anomalous Floquet chiral TSC phase in figure 5. It is found that there exist four (two pairs of) edge modes (near the two edges $n = 0$ and 100) in the energy gap at $E = 0$, which are respectively given by the red and black lines. One pair lies near $k_y = 0$, the other lies near $k_y = \pi$. Each mode has a left- or right-shifted chirality, e.g. the one (the red line) near $k_y = 0$ has the right-shifted chirality, while the one (the red line) near $k_y = \pi$ belongs to the left-shifted chirality. The similar features are shared by the edge modes in the energy gap at $E = \omega/2$. The total number of edge modes obviously satisfies equation (12). The distributed probabilities of chiral modes at $E = 0$ and $\omega/2$ for the edge modes (the red lines) at the blue circles are exhibited in figures 5(c)–(f), respectively, demonstrating they locate near the one with $n = 100$.

The anomalies-rich Floquet topological phases and corresponding phase transitions induced by g_z have the same origination as the ones by μ. The Floquet bulk energy band closes at $E = \omega/2$ with the increase of τ, leading to a new topological phase transition. Similarly, the increase of g_z also deforms the bulk energy band like μ, thus bringing about the topological phase transition at a fixed τ. However, the different features between the two tunings of static parameters (μ and g_z) observed above, originate from the combination of intrinsic (tuning τ) and different extrinsic (tuning μ and g_z) mechanisms. μ and g_z occupy different positions in the spin-dependent Hamiltonian. The former is determined by spin-independent term

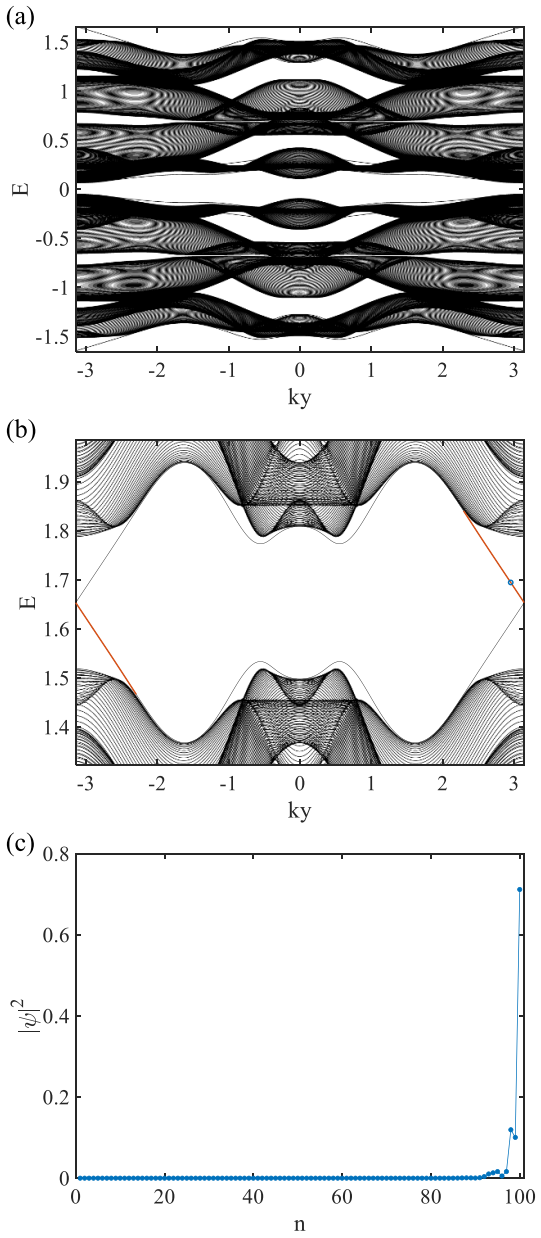

Figure 4. Edge spectrums of the anomalous Floquet chiral TSC phase $(\mathcal{C}, \mathcal{W}) = (1, -1)$ of table 1 with $\tau = 1.9$, $g_z = 0.6$, $\Delta_b = 0.4$, $\mu = 1$, $E = 0$ (a) and $\omega/2$ (b). This phase features no chiral MEM penetrating the quasi-energy gap at $E = 0$, but a pair of ones with left-shifted and right-shifted chiralities at $E = \omega/2$. The red line is the chiral modes from the edges of $n = 100$. (c) The profiles or distributed probabilities of chiral mode at the energy marked by the blue circle in (b). The momentum for the blue circle in (b) is $k_y = 3$.

$\mu\sigma_0 \bigotimes s_0$, while the latter is thoroughly dependent on spin, determined by the term $g_z\sigma_0 \bigotimes s_z$. Resultantly, the difference in energy bands induced by tuning μ and g_z, is produced.

3.3. Topological phase transitions manipulated jointly by superconducting energy gap and driving period

In this section, we display a 2D anomalous Floquet chiral TSC with Chern-number-independent chiral MEMs tuned commonly by the superconducting energy gap Δ_b and driving period τ.

Table 3 illustrates the topological phase diagram, the topological phase transition as a function of Δ_b and τ. The diagram is divided into areas 1, 2, and 3 according to the different topological phases in the high-frequency limit region. At the high-frequency limit, the phase transitions induced by Δ_b from 0.1 to 0.2 and from 1 to 1.1 are respectively due to the closure of the bulk energy band gap at $\Gamma(0,0)$ and $\mathrm{X}(\pi,0)$.

The range of Δ_b corresponding to area 1 is comparatively narrow, in which there exist five topological phases emerging sequentially, belonging to four kinds, $(2,0)$, $(1,1)$, $(0,2)$, and $(4,-2)$.

When Δ_b is slightly increased, e.g. $\Delta_b = 0.2$, area 2 just emerges. Similarly, a variety of new topological phases thoroughly different from those in area 1, start to emerge in the order of the five phases $(1,0)$, $(0,1)$,

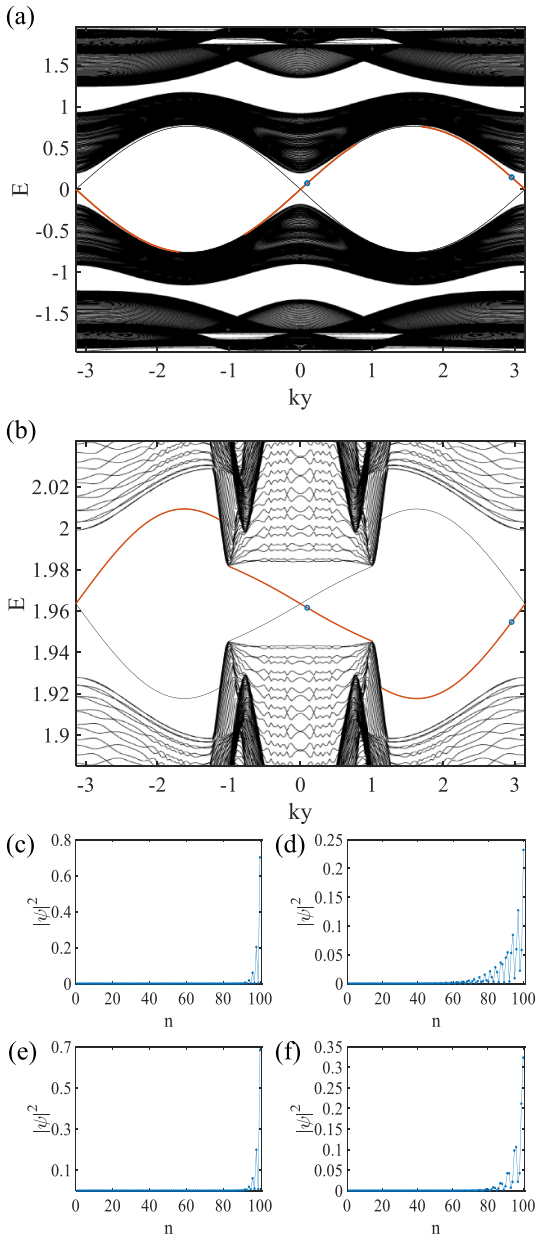

Figure 5. Edge spectrums of the anomalous Floquet chiral TSC phase $(\mathcal{C},\mathcal{W})=(0,0)$ of table 2 with $\tau=1.6$, $g_z=1$, $\Delta_b=0.4$, $\mu=0$, $E=0$ (a) and $\omega/2$ (b). This phase features two pairs of chiral edge modes at both $E=0$ and $\omega/2$ near the boundaries with $n=0$ (the black line) and 100 (the red one). The profiles or distributed probabilities (c) and (e) of chiral mode at the energy $E=0$ marked by the blue circle at $k_y=0.03\pi$ and $k_y=0.94\pi$ in (a), respectively. For (d) and (f), the same as in (c) and (e), respectively, except for $E=\omega/2$ in (b).

$(-1,2)$, $(1,0)$, and $(3,-2)$. This indicates the entirely new topological phase transitions tuned by τ and the topological transitions manipulated by Δ_b from 0.1 to 0.2 at any fixed τ between the adjacent areas. The range of Δ_b corresponding to area 2 is considerably wide. It is found that the number of topological phases appearing successively with the increase of τ can be different at different Δ_b, which could increase or decrease with the enhancement of Δ_b. This is similar to the situation for increasing μ but not for enhancing g_z. The number almost always increases with the enhancement of g_z. At different fixed Δ_b from 0.2 to 1, the former four topological phases emerging successively with the increase of τ keep unchanged, but the corresponding driving period region for each phase has a great change. The latter several topological phases appearing sequentially with the increase of τ at different fixed Δ_b are much different. In addition, the topological phase transitions modulated by Δ_b at a fixed τ including the high-frequency limit region, can appear. In this area, there exist seven new kinds of topological phases, i.e. $(0,1)$, $(1,0)$, $(-1,2)$, $(3,-2)$, $(2,-1)$, $(0,0)$ and $(-1,0)$, which are thoroughly different from those of area 1.

With the further increase of Δ_b from 1 to 1.1, area 3 starts to appear. The former three topological phases appearing sequentially thoroughly turn into new ones. Different phase transitions by τ and the phase

Table 3. The same as in table 1 except that μ is replaced by Δ_b. Here, $\mu = 0$ and $g_z = 0.6$.

τ \ Δ_b	0.1	0.2	0.3	0.4	0.5	0.6	0.7	0.8	0.9	1	1.1
0.1	2,0	1,0	1,0	1,0	1,0	1,0	1,0	1,0	1,0	1,0	-1,0
0.2											
0.3											
0.4											
0.5											
0.6											
0.7											
0.8											
0.9											
1											
1.1											
1.2										0,1	-2,1
1.3							0,1	0,1	0,1		
1.4			0,1	0,1	0,1	0,1					0,-1
1.5	1,1	0,1							2,-1	2,-1	
1.6	0,2	-1,2	-1,2	-1,2	2,-1	2,-1	2,-1	2,-1			-1,0
1.7											
1.8											
1.9		1,0	1,0	1,0	1,0	1,0	1,0	1,0	1,0	-1,0	
2	2,0										
2.1	4,-2	3,-2	3,-2	3,-2	0,1	0,1	0,1	1,0	-1,0	0,0	0,0
2.2							1,0				
2.3											
2.4			2,-1	2,-1	2,-1	3,-2	2,0	0,0	0,0		
2.5						4,-2					
2.6											

transitions by Δ_b at any fixed τ between the adjacent two areas, are resultantly induced. However, the latter two topological phases arising successively keep unchanged, thus no new phase transitions with τ are produced and the ones at few τ between the adjacent parts by Δ_b from 1 to 1.1 are exhibited. In this area, there exist only two kinds of new topological phases, i.e. $(-2, 1)$ and $(0, -1)$, which are never exhibited in the former two areas.

Although all the topological phases in table 3 are found to exhibit in tables 1 and 2, there still exist the exotic topological phase transitions, which are never exhibited in tables 1 and 2.

The above different features by the modulation of Δ_b from those by μ and g_z can be attributed to the different Hamiltonian. The location of Δ_b in it differs from those of μ and g_z, i.e. Δ_b is an off-diagonal term and closely linked to the periodic phase $e^{i\varphi(t)}$, which leads to the difference in energy bands.

Similarly, take the anomalous Floquet chiral TSC phase $(\mathcal{C}, \mathcal{W}) = (0, 2)$ at $\tau = 1.7$, $g_z = 0.6$, $\Delta_b = 0.1$, and $\mu = 0$ shown in the table 3 as an example to illustrate the bulk energy bands or the edge state of the anomalous Floquet chiral TSC phase in figure 6.

Remarkably, it is found that there exist two pairs of chiral edge modes at $E = 0$. The two modes with a left-shifted chirality from the boundary $n = 0$ are given by the black lines, while the other two modes with the right-shifted chirality from the boundary $n = 100$ are respectively presented by the red and blue lines for subsequent analyses. The same situations are for $E = \omega/2$. Similarly, equation (12) is also fulfilled by the total number of edge modes. The distributed probabilities of chiral modes at $E = 0$ and $E = \omega/2$ for the edge modes (the red and blue lines) with $k_y = 0.063$ and 2 are respectively exhibited in figures 6(c)–(f), which demonstrate they locate near the one with $n = 100$.

From the above three sections, we observe that different kinds of topological phases with τ amount to 19 by tuning μ, g_z, and Δ_b. The kind of topological phases $(-3, 1)$ by tuning μ and the three ones $(-2, 2)$, $(2, -2)$, and $(3, -1)$ by tuning g_z are respectively not exhibited in the other two situations. However, for tuning Δ_b, there are no such new topological phases.

4. Experimental feasibility

Finally, we briefly discuss the experimental feasibility. Pb(Nb) is a suitable choice for the *s*-wave SC, as it has a critical temperature T_c of 7.2 (9.5) K. By the proximity between the SC and TI, the superconductivity on the surface of the TI can be experimentally induced. The monocrystalline Bi_2Te_3 (Sb_2Te_3), which has been reported experimentally [75, 85, 86], is a possible candidate for the 3D TI, with a relatively small bulk energy gap of about 300 (100) meV. The magnetic TI can be achieved by doping Cr into Bi_2Te_3 or Sb_2Te_3 [87]. The magnetic TI-superconducting structures have already been realized experimentally, so the proposed magnetic TI sandwich Josephson structures are feasible to fabricate. In experiments, the static parameters μ, g_z, and Δ_b are tunable by varying the gate voltage V_g, the external magnetic field, and the temperature, respectively. The dynamic parameter (ω or τ) is modulated by simply changing the bias voltage V_0. The proposed Floquet setup and corresponding Floquet chiral TSC phases can be therefore experimentally realizable.

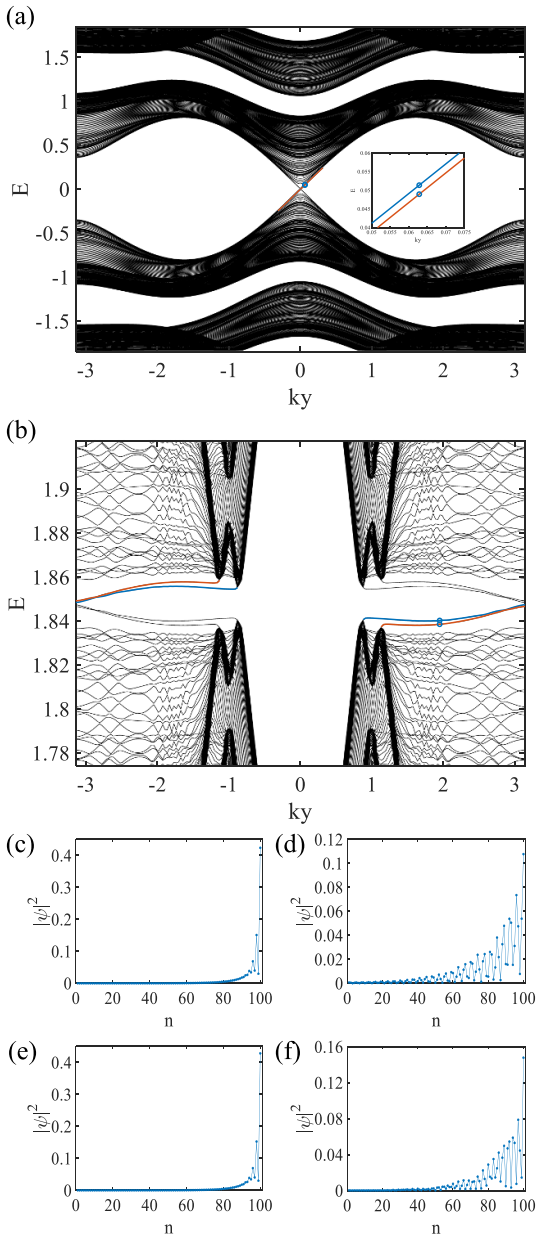

Figure 6. Edge spectrums of the anomalous Floquet chiral TSC phase $(\mathcal{C},\mathcal{W}) = (0,2)$ of table 3 with $\tau = 1.7$, $g_z = 0.6$, $\Delta_b = 0.1$, $\mu = 0$, $E = 0$ (a) and $\omega/2$ (b). This phase features two pairs of chiral edge modes at both $E = 0$ and $\omega/2$, near the boundaries with $n = 0$ (the black line) and 100 (the red and blue ones). The profiles or distributed probabilities (c) and (e) of chiral modes at $E = 0$ and $k_y = 0.063$ corresponding to the circles of the blue and red lines in (a), respectively. For (d) and (f), the same as in (c) and (e), respectively, except for $E = \omega/2$ and $k_y = 2$ in (b).

5. Summary

In summary, we study the anomalous Floquet chiral TSC phases by jointly tuning dynamic driving and static parameters, based on a magnetic TIs-superconductor sandwich Josephson hybrid structure. A static bias voltage applied across the top and bottom superconducting layers provides a periodic driving. By jointly tuning dynamic driving (τ) and static (μ, g_z, and Δ_b) parameters, a variety of anomalies-rich Floquet TSC phases are exhibited. There exist four features as follows. (1) In the low frequency ω region, for different μ, different novel Floquet topological phase transitions can occur sequentially with τ increased. The processes are accompanied by the closure of the energy gap at the high-symmetry point $E = \omega/2$ of the bulk energy bands. The same features are for g_z and Δ_b. (2) For μ, there always exist several special values, at two any adjacent values of which, the corresponding topological phases appearing successively with the increase of τ could be thoroughly different. A series of topological phase transitions in the whole τ region tuned by μ are indicated as well. The same features exhibit for g_z and Δ_b. During all the phase transitions, the closure of the bulk band gap at $E = 0$ occurs simultaneously at the high-symmetry points of Brillouin zone. (3) The

numbers of the topological phases arising successively tuned by τ may both increase or decrease with the enhancement of the two parameters μ and Δ_b, while the number is basically increased with g_z. (4) Jointly tuning τ and μ (g_z) can have its own unique TSC phases.

The features among the tunings of three static parameters are different, originating from the combination of intrinsic and different extrinsic mechanisms. The family of anomalous Floquet TSC phases induced by the tunings is considerably enriched.

Here, it is worth noting that in the phase diagram, the computation time for a single point is approximately one hour. To achieve a continuous phase diagram, the order of magnitude for the interval values of both the periodic driving and static parameters is 10^{-2}. Take table 1 as an instance, a complete phase diagram would necessitate 25 351 points, indicating more than 1000 days of computational time, an unfeasible duration for us. A practical approach to obtain more detailed topological phase information is to select a region of interest in the parameter space based on the present topological phase diagram (e.g. table 1). Taking the phase transition boundary region with $\tau = (1.6, 1.7)$ and $\mu = (0.3, 0.4)$ as an example, the complete calculation would only require 144 points, which could be completed in 6 days. If the calculation is deployed on a high-performance work cluster or supercomputer, the time will be further reduced. Such an operation not only saves time but also ensures the accuracy and reliability of the results. Moreover, it does not affect our qualitative conclusions and characteristics, which are thoroughly determined by the properties of the topological invariants.

Data availability statement

All data that support the findings of this study are included within the article (and any supplementary files).

Acknowledgment

The authors would like to thank Prof. Rui-Xing Zhang from the University of Tennessee, Knoxville for the tremendous help. This work was supported by the National Natural Science Foundation of China (Grant Nos. 12274232, 12074332, and 12274233).

ORCID iDs

Donghao Wang https://orcid.org/0009-0008-1118-9079
Zixuan Ding https://orcid.org/0009-0003-7455-0937
Yongchun Tao https://orcid.org/0000-0001-5539-3815
Jingguo Hu https://orcid.org/0000-0003-3829-5177

References

[1] Liu C-X, Zhang S-C and Qi X-L 2016 The quantum anomalous hall effect: theory and experiment *Annu. Rev. Condens. Matter Phys.* **7** 301
[2] Haldane F D M 1988 Model for a quantum hall effect without landau levels: condensed-matter realization of the "parity anomaly" *Phys. Rev. Lett.* **61** 2015
[3] Kane C L and Mele E J 2005 Z_2 topological order and the quantum spin hall effect *Phys. Rev. Lett.* **95** 146802
[4] Bernevig B A and Zhang S-C 2006 Quantum spin hall effect *Phys. Rev. Lett.* **96** 106802
[5] Hasan M Z and Kane C L 2010 Colloquium: topological insulators *Rev. Mod. Phys.* **82** 3045
[6] Qi X-L and Zhang S-C 2011 Topological insulators and superconductors *Rev. Mod. Phys.* **83** 1057
[7] Read N and Green D 2000 Paired states of fermions in two dimensions with breaking of parity and time-reversal symmetries and the fractional quantum hall effect *Phys. Rev.* B **61** 10267
[8] Kitaev A 2001 Unpaired Majorana fermions in quantum wires *Phys.-Usp.* **44** 131
[9] Lutchyn R M, Sau J D and Das Sarma S 2010 Majorana fermions and a topological phase transition in semiconductor-superconductor heterostructures *Phys. Rev. Lett.* **105** 077001
[10] Sarma S D, Freedman M and Nayak C 2015 Majorana zero modes and topological quantum computation *npj Quantum Inf.* **1** 1
[11] Lutchyn R M, Bakkers E P A M, Kouwenhoven L P, Krogstrup P, Marcus C M and Oreg Y 2018 Majorana zero modes in superconductor-semiconductor heterostructures *Nat. Rev. Mater.* **3** 52
[12] Prada E, San-Jose P, de Moor M W, Geresdi A, Lee E J, Klinovaja J, Loss D, Nygãard J, Aguado R and Kouwenhoven L P 2020 From Andreev to Majorana bound states in hybrid superconductor–semiconductor nanowires *Nat. Rev. Phys.* **2** 575
[13] Ivanov D A 2001 Non-Abelian statistics of half-quantum vortices in *p*-wave superconductors *Phys. Rev. Lett.* **86** 268
[14] Sarma S D, Freedman M and Nayak C 2006 Topological quantum computation *Phys. Today* **59** 7
[15] Kitaev A Y 2003 Fault-tolerant quantum computation by anyons *Ann. Phys.* **303** 2
[16] Stern A 2010 Non-Abelian states of matter *Nature* **464** 187
[17] Nayak C, Simon S H, Stern A, Freedman M and Das Sarma S 2008 Non-Abelian anyons and topological quantum computation *Rev. Mod. Phys.* **80** 1083
[18] Kitagawa T, Berg E, Rudner M and Demler E 2010 Topological characterization of periodically driven quantum systems *Phys. Rev.* B **82** 235114

[19] Jiang L, Kitagawa T, Alicea J, Akhmerov A R, Pekker D, Refael G, Cirac J I, Demler E, Lukin M D and Zoller P 2011 Majorana fermions in equilibrium and in driven cold-atom quantum wires *Phys. Rev. Lett.* **106** 220402
[20] Rudner M S, Lindner N H, Berg E and Levin M 2013 Anomalous edge states and the bulk-edge correspondence for periodically driven two-dimensional systems *Phys. Rev.* X **3** 031005
[21] Nathan F and Rudner M S 2015 Topological singularities and the general classification of Floquet-Bloch systems *New J. Phys.* **17** 125014
[22] Yao S, Yan Z and Wang Z 2017 Topological invariants of floquet systems: general formulation, special properties and floquet topological defects *Phys. Rev.* B **96** 195303
[23] Peng Y and Refael G 2019 Floquet second-order topological insulators from nonsymmorphic space-time symmetries *Phys. Rev. Lett.* **123** 016806
[24] Perez-Piskunow P M, Foa Torres L E F and Usaj G 2015 Hierarchy of Floquet gaps and edge states for driven honeycomb lattices *Phys. Rev.* A **91** 043625
[25] Morimoto T, Po H C and Vishwanath A 2017 Floquet topological phases protected by time glide symmetry *Phys. Rev.* B **95** 195155
[26] Molignini P, Chen W and Chitra R 2020 Generating quantum multicriticality in topological insulators by periodic driving *Phys. Rev.* B **101** 165106
[27] Mondal D, Ghosh A K, Nag T and Saha A 2023 Topological characterization and stability of Floquet Majorana modes in Rashba nanowires *Phys. Rev.* B **107** 035427
[28] Iorsh I V, Sedov D D, Kolodny S A, Sinitskiy R E and Kibis O V 2024 Floquet engineering of the Lifshitz phase transition in the Hubbard model *Phys. Rev.* B **109** 035104
[29] Ghosh A K, Nag T and Saha A 2023 Time evolution of Majorana corner modes in a Floquet second-order topological superconductor *Phys. Rev.* B **107** 035419
[30] Shi K, Zhang X and Zhang W 2024 Floquet topological phases with large winding number (arXiv:2401.01250)
[31] Li T and Hu H 2023 Floquet non-Abelian topological insulator and multifold bulk-edge correspondence *Nat. Commun.* **14** 6418
[32] Wu H and An J-H 2023 Hybrid-order topological odd-parity superconductors via Floquet engineering *Phys. Rev.* B **107** 235132
[33] Adiyatullin A F, Upreti L K, Lechevalier C, Evain C, Copie F, Suret P, Randoux S, Delplace P and Amo A 2023 Topological properties of floquet winding bands in a photonic lattice *Phys. Rev. Lett.* **130** 056901
[34] Zhou L and Zhang D-J 2023 Non-hermitian floquet topological matter-a review *Entropy* **25** 1401
[35] Zhou L, Gu Y and Gong J 2021 Dual topological characterization of non-Hermitian Floquet phases *Phys. Rev.* B **103** L041404
[36] Zhou L and Han W 2022 Driving-induced multiple $\mathcal{PT}$-symmetry breaking transitions and reentrant localization transitions in non-Hermitian Floquet quasicrystals *Phys. Rev.* B **106** 054307
[37] Pan J and Zhou L 2020 Non-Hermitian Floquet second order topological insulators in periodically quenched lattices *Phys. Rev.* B **102** 094305
[38] Zhou L 2020 Non-Hermitian Floquet topological superconductors with multiple Majorana edge modes *Phys. Rev.* B **101** 014306
[39] Liu X, Tan S, Wang Q-H, Zhou L and Gong J 2022 Floquet band engineering with Bloch oscillations *Phys. Rev.* B **106** 224309
[40] Drüeke H, Meschede M and Bauer D 2023 Steering edge currents through a Floquet topological insulator *Phys. Rev. Res.* **5** 023056
[41] Zhou L 2022 Generating many Majorana corner modes and multiple phase transitions in Floquet second-order topological superconductors *Symmetry* **14** 2546
[42] Wu H, Wu S and Zhou L 2023 Floquet topological superconductors with many Majorana edge modes: topological invariants, entanglement spectrum and bulk-edge correspondence *New J. Phys.* **25** 083042
[43] Vu D, Zhang R-X, Yang Z-C and Das Sarma S 2021 Superconductors with anomalous Floquet higher-order topology *Phys. Rev.* B **104** L140502
[44] Ghosh A K, Nag T and Saha A 2021 Floquet second order topological superconductor based on unconventional pairing *Phys. Rev.* B **103** 085413
[45] Ghosh A K, Nag T and Saha A 2021 Floquet generation of a second-order topological superconductor *Phys. Rev.* B **103** 045424
[46] Oka T and Kitamura S 2019 Floquet engineering of quantum materials *Annu. Rev. Condens. Matter Phys.* **10** 387
[47] Mori T 2023 Floquet states in open quantum systems *Annu. Rev. Condens. Matter Phys.* **14** 35
[48] Harper F, Roy R, Rudner M S and Sondhi S 2020 Topology and broken symmetry in floquet systems *Annu. Rev. Condens. Matter Phys.* **11** 345
[49] Wintersperger K, Braun C, Ünal F N, Eckardt A, Liberto M D, Goldman N, Bloch I and Aidelsburger M 2020 Realization of an anomalous Floquet topological system with ultracold atoms *Nat. Phys.* **16** 1058
[50] Jotzu G, Messer M, Desbuquois R, Lebrat M, Uehlinger T, Greif D and Esslinger T 2014 Experimental realization of the topological Haldane model with ultracold fermions *Nature* **515** 237
[51] Cooper N R, Dalibard J and Spielman I B 2019 Topological bands for ultracold atoms *Rev. Mod. Phys.* **91** 015005
[52] Mukherjee S, Spracklen A, Valiente M, Andersson E, Öhberg P, Goldman N and Thomson R R 2017 Experimental observation of anomalous topological edge modes in a slowly driven photonic lattice *Nat. Commun.* **8** 13918
[53] Afzal S, Zimmerling T J, Ren Y, Perron D and Van V 2020 Realization of anomalous floquet insulators in strongly coupled nanophotonic lattices *Phys. Rev. Lett.* **124** 253601
[54] Mukherjee S and Rechtsman M C 2020 Observation of Floquet solitons in a topological bandgap *Science* **368** 856
[55] Maczewsky L J, Zeuner J M, Nolte S and Szameit A 2017 Observation of photonic anomalous Floquet topological insulators *Nat. Commun.* **8** 13756
[56] Segev M and Bandres M A 2021 Topological photonics: where do we go from here? *Nanophotonics* **10** 425
[57] Ozawa T *et al* 2019 Topological photonics *Rev. Mod. Phys.* **91** 015006
[58] Kirsch M S, Zhang Y, Kremer M, Maczewsky L J, Ivanov S K, Kartashov Y V, Torner L, Bauer D, Szameit A and Heinrich M 2021 Nonlinear second-order photonic topological insulators *Nat. Phys.* **17** 995
[59] Ivanov S K, Kartashov Y V, Heinrich M, Szameit A, Torner L and Konotop V V 2021 Topological dipole Floquet solitons *Phys. Rev.* A **103** 053507
[60] Rechtsman M C, Zeuner J M, Plotnik Y, Lumer Y, Podolsky D, Dreisow F, Nolte S, Segev M and Szameit A 2013 Photonic Floquet topological insulators *Nature* **496** 196
[61] Hafezi M, Mittal S, Fan J, Migdall A and Taylor J M 2013 Imaging topological edge states in silicon photonics *Nat. Photon.* **7** 1001
[62] Peng Y-G, Qin C-Z, Zhao D-G, Shen Y-X, Xu X-Y, Bao M, Jia H and Zhu X-F 2016 Experimental demonstration of anomalous Floquet topological insulator for sound *Nat. Commun.* **7** 13368
[63] Fleury R, Khanikaev A B and Alù A 2016 Floquet topological insulators for sound *Nat. Commun.* **7** 11744

[64] Zhang R-X and Das Sarma S 2021 Anomalous floquet chiral topological superconductivity in a topological insulator sandwich structure *Phys. Rev. Lett.* **127** 067001
[65] Seroussi I, Berg E and Oreg Y 2014 Topological superconducting phases of weakly coupled quantum wires *Phys. Rev.* B **89** 104523
[66] Stanescu T D, Sau J D, Lutchyn R M and Das Sarma S 2010 Proximity effect at the superconductor–topological insulator interface *Phys. Rev.* B **81** 241310
[67] Potter A C and Lee P A 2011 Engineering a $p+ip$ superconductor: Comparison of topological insulator and Rashba spin-orbit-coupled materials *Phys. Rev.* B **83** 184520
[68] Stoudenmire E M, Alicea J, Starykh O A and Fisher M P 2011 Interaction effects in topological superconducting wires supporting Majorana fermions *Phys. Rev.* B **84** 014503
[69] Mashkoori M, Moghaddam A G, Hajibabaee M H, Black-Schaffer A M and Parhizgar F 2019 Impact of topology on the impurity effects in extended *s*-wave superconductors with spin-orbit coupling *Phys. Rev.* B **99** 014508
[70] Zhang F, Kane C L and Mele E J 2013 Time-reversal-invariant topological superconductivity and Majorana Kramers pairs *Phys. Rev. Lett.* **111** 056402
[71] Zhou B-Z, Xu D-H and Zhou B 2017 Majorana zero modes in a ladder of density-modulated Kitaev superconductor chains *Phys. Lett.* A **381** 2426
[72] Plekhanov K, Ronetti F, Loss D and Klinovaja J 2020 Hinge states in a system of coupled Rashba layers *Phys. Rev. Res.* **2** 013083
[73] Hung H-H, Ghaemi P, Hughes T L and Gilbert M J 2013 Vortex lattices in the superconducting phases of doped topological insulators and heterostructures *Phys. Rev.* B **87** 035401
[74] Hosur P, Ghaemi P, Mong R S K and Vishwanath A 2011 Majorana modes at the ends of superconductor vortices in doped topological insulators *Phys. Rev. Lett.* **107** 097001
[75] Tokura Y, Yasuda K and Tsukazaki A 2019 Magnetic topological insulators *Nat. Rev. Phys.* **1** 126
[76] Sacramento P D 2015 Charge and spin edge currents in two-dimensional Floquet topological superconductors *Phys. Rev.* B **91** 214518
[77] Sato M and Fujimoto S 2009 Topological phases of noncentrosymmetric superconductors: edge states, Majorana fermions and non-Abelian statistics *Phys. Rev.* B **79** 094504
[78] Sacramento P D, Araújo M A N and Castro E V 2014 Hall conductivity as bulk signature of topological transitions in superconductors *Europhys. Lett.* **105** 37011
[79] Oka T and Aoki H 2009 Photovoltaic hall effect in graphene *Phys. Rev.* B **79** 081406
[80] Xiao D, Chang M-C and Niu Q 2010 Berry phase effects on electronic properties *Rev. Mod. Phys.* **82** 1959
[81] Bott R and Seeley R 1978 Some remarks on the paper of callias *Commun. Math. Phys.* **62** 235
[82] Carpentier D, Delplace P, Fruchart M and Gawędzki K 2015 Topological index for periodically driven time-reversal invariant 2D systems *Phys. Rev. Lett.* **114** 106806
[83] Goldman N and Dalibard J 2014 Periodically driven quantum systems: effective hamiltonians and engineered gauge fields *Phys. Rev.* X **4** 031027
[84] Yu J, Zhang R-X and Song Z-D 2021 Dynamical symmetry indicators for Floquet crystals *Nat. Commun.* **12** 5985
[85] Ando Y 2013 Topological insulator materials *J. Phys. Soc. Japan* **82** 102001
[86] Cava R J, Ji H, Fuccillo M K, Gibson Q D and Hor Y S 2013 Crystal structure and chemistry of topological insulators *J. Mater. Chem.* C **1** 3176
[87] Chang C-Z *et al* 2013 Thin films of magnetically doped topological insulator with carrier-independent long-range ferromagnetic order *Adv. Mater.* **25** 1065